Laser-Induced Ignition in Solid-State Combustion

The ignition process of condensed-phase combustion by a laser is studied experimentally as well as numerically. Numerical simulations are performed in one, two and three spatial dimensions, and are compared with the experimental observations. The effects of energy-dissipative mechanisms, such as melting and ablation due to laser irradiation and the effects of laser power output fluctuations, are also studied. We find that the ignition process depends mainly on the energy deposited in the system. The time leading up to ignition is longer for higher light fluxes keeping the average laser power constant, since a larger fraction of the energy is reradiated from the heated surface or consumed during the process of material removal.

P. Dimitriou, V. Hlavacek
Department of Chemical Engineering
State University of New York
Buffalo, NY 14260

Steven M. Valone, Robert G. Behrens
Los Alamos National Laboratory
Materials Science & Technology Division
Los Alamos, NM 87545

G. P. Hansen, J. L. Margrave
Department of Chemistry
Rice University
Houston, TX 77251

Introduction

Combustion in condensed systems is an efficient method of synthesis of many high-performance ceramic materials, such as carbides, borides, nitrides, and silicides. The process utilizes the heat released by an exothermic reaction between the precursor components. After ignition of the exothermic reaction by an energy source with a short-term service, a reaction front forms which is self-sustaining and propagates throughout the unreacted sample as long as fresh material is available. This process, sometimes referred to as self-propagating high-temperature synthesis (SHS), is a unique technology for preparing advanced ceramic materials. Its major advantages over conventional processes are: fast processing of the material, self-purification, and generation of temperatures in excess of 2,000 K. Therefore, an expensive furnace is not necessary for this process. Initiation of such processes is obtained by conductive heat exchange or by a flow of radiant energy (Merzhanov and Averson, 1971).

The ignition temperature of certain solid-state combustion reactions (Ti + C, Zr + C, etc.) is very high, and powerful ignition systems must be used. To initiate such types of reactions, two energy sources can be used: 1) laser beam and 2) electron beam. In this paper, we analyze the ignition characteristics produced by a laser beam. Initiation of SHS reactions by power light fluxes has been studied experimentally (Phung and Hardt, 1974; Korotkevich et al., 1981; Mikheev et al., 1968; Baranovskii, 1983; Vidavskii et al., 1974; Sotvbun et al., 1972), as well as theoretically (Merzhanov and Averson, 1971; Phung and Hardt, 1974; Assorskii and Leipunskii, 1980; Zarko and Kiskin, 1980; Vilyunov, 1966). In the theoretical studies, the ignition problem was studied in one dimension, because of the very long computation times required in the numerical simulation in two and three dimensions.

The aim of the present work is to explore laser-induced ignition of SHS reactions in the higher dimensions and to make comparisons with experiments wherever possible. By incorporating mesh adaption techniques, the numerical simulations can deal with aspects of all three spatial dimensions. Whenever it is appropriate, issues are dealt with in one and/or two spatial dimensions. Also studied are the following effects of energy-dissipative mechanisms: melting and ablation due to laser irradiation power profile; laser power output fluctuations; and focusing location on the irradiated surface on the ignition time delay.

In combustion systems, the ignition time is the minimum amount of time that the heat source—in this case a laser beam— is allowed to interact with the sample which results in a sustained reaction. This is the definition used in computing ignition times from the simulations. In the experiments, temperature histories are recorded from pyrometry data taken from several locations on the sample surface. Signatures of the ignition process in the form of abrupt changes in the temperature traces are used to indicate ignition. Consequently, the experimental ignition times are upper bounds to the rigorous ignition times. This study is carried out to assess the aptness of such signatures for ignition phenomena as well.

Experimental Study

The reactions studied are Ti+C and Zr+C. The samples used have cylindrical geometry and consist of stoichiometric mixtures of the elemental powders pressed at 1.38×10^8 to 2.76×10^8 Pa. The green compacts are 40–60% of theoretical density. The distribution of porosity between the two components is unknown at this time.

The experimental procedure (Hansen et al., 1987; Fredin et al., 1986) involves the use of split-frame high-speed photography together with optical pyrometry to obtain kinetic and temperature data during the course of laser heating and reaction. The experimental arrangement used for the high-speed photography/optical pyrometry experiments is shown in Figure 1. A 120° section is removed from the mount ring to allow viewing of the lateral surface during an experiment. Only six 5-mil tungsten wire pins are in contact with the sample. The sample mount ring is attached to a three-direction translation stage so that the sample can be positioned as desired. A video camera, positioned to view the sample front surface, is used to assist in alignment of the sample prior to the experiment. During the experiment, the video system is convenient for observing the behavior of the sample in the laser-heated region of the sample front surface. After mounting the sample, the sample chamber is evacuated to about 26.6 Pa for 180–300 seconds and then backfilled with argon to 1,333 Pa.

The laser used in these experiments consists of a HELIOS HF-DF *cw* laser operating in the DF multiline (line center 3 μm), TEM_{∞} mode. The power output of this laser is nominally 100 W. The laser is focused using a CsBr, 0.5 m focal length lens, enters the vacuum chamber through a sapphire window, and impinges on the front surface of the sample. The sample is positioned in such a way that the front surface of the pellet is at the focal point of the lens. The laser beam and the sample are coaxial.

Three mirrors inside the vacuum chamber reflect images of the front, back and side surfaces of the sample to three nesting mirrors above the chamber. The high-speed camera (NAC, model E-10) views images of the sample from the nesting mirrors. The laser shutter is triggered to open when the high-speed camera is up to full speed. The closure time of the laser shutter is preprogrammed in the data acquisition computer prior to an experiment.

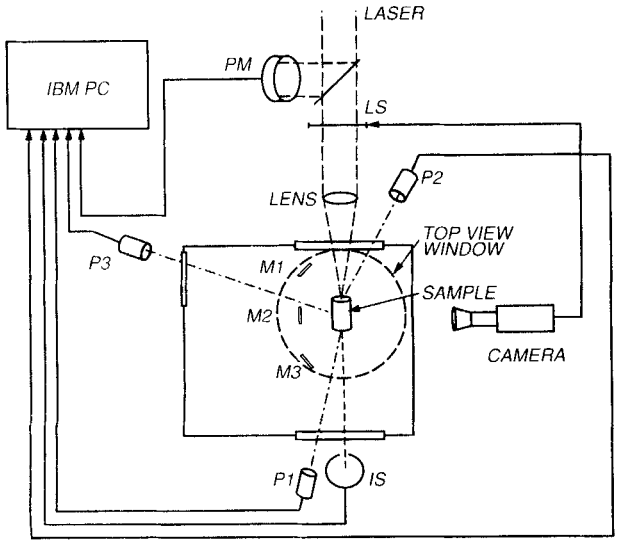

Figure 1. Experimental arrangement.

PM = photomultiplier
LS = laser shutter
P1,P2,P3 = pyrometers
M1,M2,M3 = mirrors
IS = interrupt switch

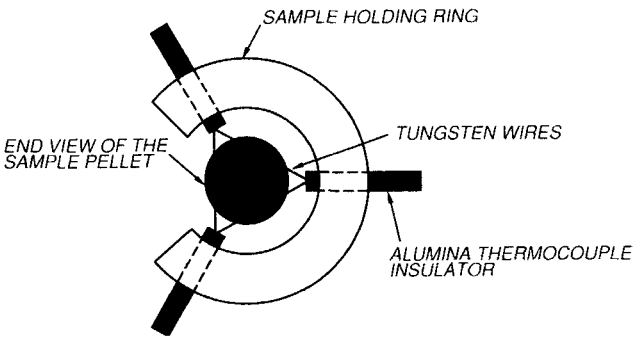

Figure 2. Device used to mount samples.

Concomitant with the high-speed photographing monitoring of the sample, the temperatures of the front, side and back surfaces of the sample are monitored using pyrometers. For the front and side surface temperature measurements, two Thermogauge single-color pyrometers (P2, P3) are used ($\lambda_{max} = 0.8$ μm and $\lambda_{max} = 1.5$ μm, respectively). An IRCON pyrometer (P1:$\lambda_{max} = 0.75$ and 1.05 μm) is used to monitor the back surface temperature. Data acquisition by the pyrometers is preprogrammed to begin 0.5 s prior to the opening of the laser shutter.

To determine the temporal occurrence and magnitude of burnthrough, an integrating sphere is situated outside the vacuum chamber on the laser beam axis. The laser power is monitored continuously during an experiment using a Scientech power meter. The sample pellet reflectance of laser light is measured in an independent experiment by placing a calibrated integrating sphere in front of the sample and monitoring the temporal output of the detector in that sphere during the entire course of a combustion experiment. Using a modified version of the device shown in Figure 2, the temporal profiles of the sample pellet reflectances are measured during this entire course of laser heating. To perform these experiments, an integrating sphere, calibrated using a diffuse gold film, is placed at the front surface of the sample. During these experiments, photography data and lateral surface temperature data are not taken. During all experiments, systematic variations in the pellet and laser heating parameters are performed: pellet mass, the length-to-diameter ratio of the pellet, the pellet density, the laser focal spot diameter, and the laser pulse duration. The ranges for these parameters are given in Table 1.

Table 1. Pellet and Laser Heating Parameters

Parameters	Range
Pellet mass (kg)	0.05–1.30
Pellet *L/d* ratio	0.2–2.2
Pellet density ($kg/m^3 \times 10^3$)	1.9–5.7
Laser spot area ($m^2 \times 10^{-6}$)	0.85–1.1
Average laser power (W)	77–107
Laser pulse duration (s)	1.0–52.0

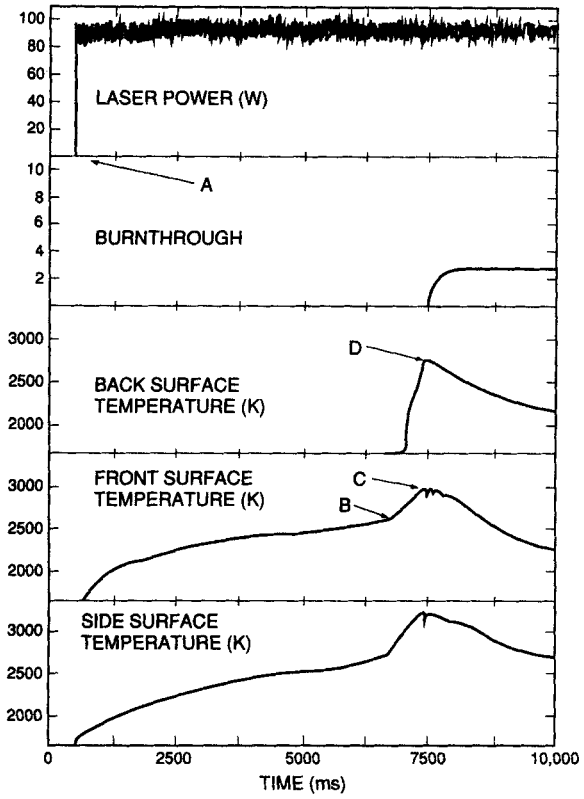

Figure 3. Pyrometry data for a Ti+C reaction where the laser impinges on the sample during the entire course of reaction.

Laser power (W) is given in the top trace; burnthrough (arbitrary units) in the second trace; and back, front and side surface temperatures (K) in the bottom three traces.

Experimental Observation and Results

The ignition time of the pellet is determined as the temporal difference between the opening of the laser shutter (Point A, Figure 3) and the cusp on the front surface temperature trace (Point B). Typical ignition times and temperatures are observed to be on the order of 0.4 seconds, and 2,400 K, respectively. Detailed comparison of experimental ignition times with those of the numerical values will be made below.

In experiments where the laser spot diameter is on the order of 5% of the sample diameter or less, sample heating is essentially linear in time between the initial temperature rise at the opening of the laser shutter and ignition. On the other hand, for larger spot diameters, heating of the sample follows a square root of time behavior before ignition (Figure 4, Front Surface Trace). Also, for these larger laser spot diameters, it is not usually possible to distinguish precisely when ignition occurs, due to the absence of the ignition cusp on the front surface pyrometry trace. For these cases, the maximum duration of the ignition induction period is estimated by the time lapse between the opening of the laser shutter and the initial rise in temperature on the back surface pyrometry trace.

A point of interest concerns the magnitude of the rise in temperature on the front surface following ignition. Typically, the value is on the order of 600–800 K, considerably less than that expected for adiabatic combustion (3,200 K for TiC, 3,400 K for ZrC). On the other hand, the back surface temperature, which rises rapidly following ignition, indicates a combustion temperature considerably closer to, but still 800–900 degrees less than, the calculated value. Average ignition and combustion temperatures for Ti+C and Zr+C are given in Table 2, as are the average front surface temperature jumps following ignition. The numbers given in parentheses are the coefficients of variation for each value shown and are calculated from a population number of 20. These results indicate that extensive preignition reaction (50% in front third of sample) occurs. On the other hand, the reactions are only 75% adiabatic at the maximum combustion temperatures. Considerable radiative heat loss occurs during combustion. It is clear from the video monitor, as well as the temperature profiles, that melting of the pellet around the laser-heated spot starts early in the experiment. In fact, the measured front surface temperatures exceed the melting temperatures of the metal, 1,933 K for Ti and 3,125 K for Zr, within the first 10–20% of the induction period. This result points to the fact that the molten metal plays a substantial role in the ignition mechanism.

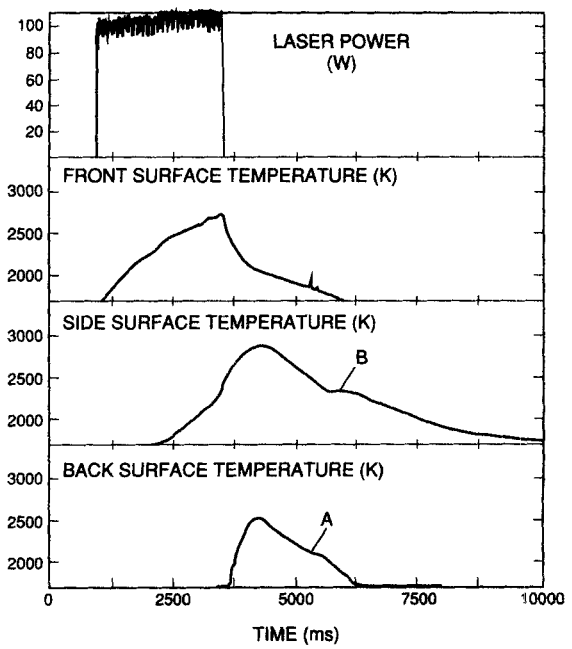

Figure 4. Pyrometry data for a Ti+C reaction where the laser shutter is closed at ignition.

Shown in Figure 4 are the temperature data for an experiment where the laser shutter is closed at the point of ignition. Of notable interest are the secondary temperature bumps on the back and side surface traces indicated by the letters A and B, respectively. For this case, it appears that after the combustion

Table 2. Average Ignition and Combustion Temperatures for Ti + C and Zr + C

Reaction	Ignition Temp.** K	Comb. Temp.† K	Temp. Jump‡ K
Ti + C*	2,326 (15)	2,398 (18)	779 (37)
Zr + C*	2,568 (11)	2,507 (15)	677 (29)

*Parenthetic values give the coefficient of variation.
**Front surface.
†Back surface.
‡At ignition.

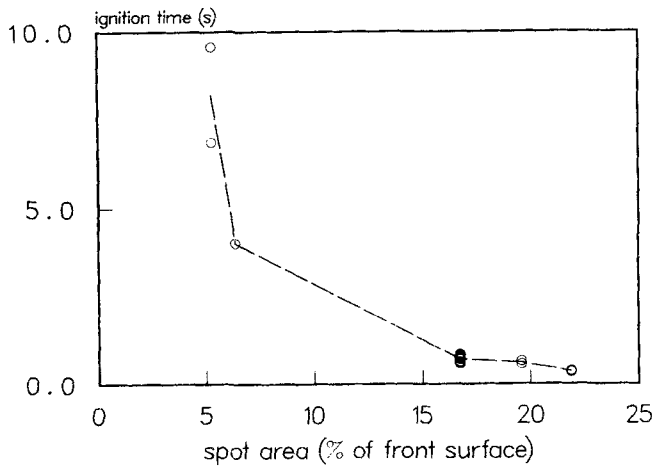

Figure 5. Ignition induction time as a function of front surface coverage by the laser spot for Ti+C.
Peak power densities vary between 8.6×10^7 and 12.0×10^7 W/m^2.

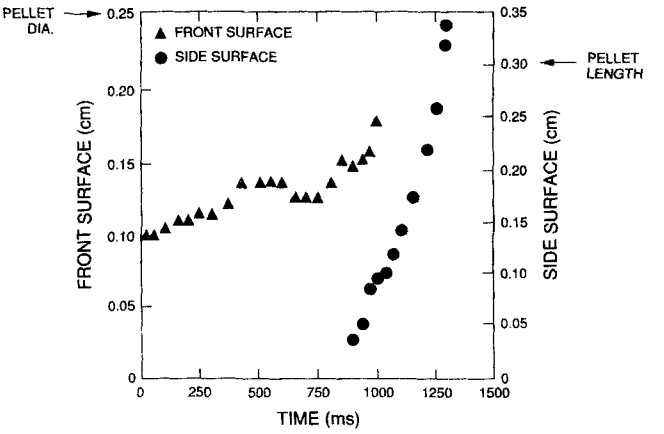

Figure 6. Typical data from analysis of a high-speed film.
The left vertical axis gives the diameter of the heat wave as it covers the front surface. The right vertical axis gives the position of the heat wave as it passes down the pellet axis.

wave passes through the sample, it propagates back toward the front surface. The secondary combustion wave could be supported only if substantial unreacted material remains after initial combustion. The high speed of the combustion wave and extensive radiation losses at the pellet surfaces are considered primary factors that lead to lowered product conversions and the low adiabaticity of the reactions.

The point course data of Figure 5 show ignition induction time as a function of laser spot diameter relative to the sample diameter, expressed as a percentage. The induction times are measured from the pyrometry data. The data plotted in the figure are taken from the results of the Ti+C reactions. The line drawn through the data is not meant to be interpreted as a fit; rather, it indicates an average that was done for purposes of illustration. Three observations are made here: 1. The induction time is relatively constant, ~1 s, between 10% and 22% coverage of the front surface by the laser spot. 2. Below 10%, the induction time increases dramatically. To achieve the smaller laser spot diameters, tighter focusing of the laser is required. This leads to higher flux of laser radiation, making it lose more power to ablation of the sample. 3. No data are given for spot sizes greater than 22% of the front surface. At some point, larger spot sizes will result in too much laser light being lost in the Gaussian tails of the laser beam, which miss the pellet altogether, so that ignition will not be observed. Further experiments at larger spot diameters will be necessary to determine this point. As will be seen later, some light is shed on this point from the numerical calculations which predict an optimum spot size of 75% for this system.

Figure 6 illustrates results from a high-speed film analysis. The left vertical axis gives the diameter of the heat wave as it propagates across the front surface from the laser spot. Likewise, the right vertical axis shows the scale for the position of the heat wave as it passes down the axis of the pellet. Several points are notable concerning this figure.

1. As the combustion wave propagates down the pellet axis, expansion of the sample occurs, so that, from the figure, it would appear that the combustion wave propagates further than the pellet length. During analysis of the films, it is not visibly apparent that the sample size is increasing. Only after plotting the data on a graph such as that shown in Figure 6 does it become apparent that swelling of the sample occurs during combustion.

2. It is possible to estimate ignition times from the photography data by extrapolating the last few, approximately linear, side surface data points back to the time axis. This gives ignition times, which are consistent with those obstained from the temperature data—within 15%.

3. The side surface data never becomes linear, even as the combustion wave reaches the end of the pellet. Rather, the combustion wave continues to accelerate in a parabolic manner. This observation indicates that the reaction does not achieve a steady-state combustion rate. This is attributable to the small sizes of samples used, and larger samples are expected to allow steady-state combustion to be achieved.

4. Side surface data are obtainable *before* the combustion wave consumes the front surface. To be registered on the film, any section of the sample must be at a temperature of 1,000 K or higher. Thus, before ignition occurs, the front 25 to 33% of the sample is heated to temperatures above 0.4 T_{ign}. This result is consistent with the fact that extensive preignition reaction occurs as noted above.

An interesting phenomenon associated with laser heating of the samples is noteworthy. From the side view images in the high-speed films, it is observed that particle ejection from the laser-heated spot occurs during the induction period. Approximately 5,000–10,000 particles per second, ranging in diameter form submicron to 1 mm are ejected in a roughly cosine-squared spatial distribution, having velocities on the order of 300 m/s and temperatures on the order of 3,000 K. A simple calculation indicates the extent of energy loss through the ablation process. The total kinetic energy of the material leaving the surface is on the order of 0.1 W, which is inconsequential. On the other hand, the radiated power of the ejected particles can be substantial. For instance, a particle with diameter on the order of 10^{-6} m. A particle with a diameter on the order of 10^{-3} m radiates 3 W. To accurately determine the radiated losses occurring as a result of particle ejection, the size and temperature distributions of the particles must be known. From the rough calculation, however, it is possible to estimate that as much as 10 W of laser power is lost to radiation by the particles.

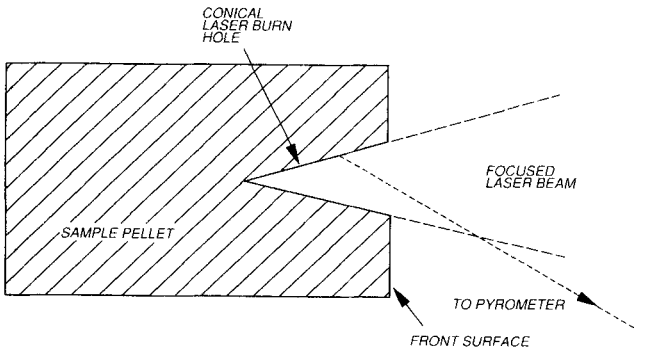

Figure 7. Cross-sectional schematic of a typical sample after extensive ablation from the laser-heated spot.

The result of melting, vaporization and particle ejection is that a conical hole is ablated in the sample during the experiment (Figure 7). In some instances (Figure 3) a hole is bored through the pellet as the combustion wave reaches the back surface. In these cases, it is clear that vaporization is assisted by the additional heat of reaction. Vaporization ceases as the refractory product forms and cools from the melt after propagation of the combustion wave.

Theoretical Analysis

The aim of the theoretical analysis is to predict the ignition temperatures and the ignition time delays for fast-induced ignition in SHS. The basic tool for the theoretical investigation of solid-state ignition is the solution of the nonlinear heat conduction equations.

Model Formulation and Numerical Integration

The formulation of the model is based on the following assumptions:

- A heterogeneous mixture of solid powders A and B behaves as an isotropic mixture.
- The temperature dependence of the reaction rate constant can be expressed in the Arrhenius form.
- Heat conduction in the solid phase can be described in terms of the Fourier Law.
- Mass diffusion of the solid reactants or products is ignored.
- All physical properties (density, heat capacity, and effective thermal conductivity) are assumed constant.
- The reaction is strongly exothermic.
- The reaction, $A(s)+B(s)\rightarrow P(s)$, is considered first order with respect to the limiting reactant A.
- No depth of penetration of the laser beam is considered (i.e., the laser is treated as a surface heat source).

Based on the above assumptions, the equations, which describe the laser-induced ignition in cylindrical coordinates, are as follows:

Energy balance:

$$\rho C_p\, \partial T/\partial t = \lambda[\partial^2 T/\partial z^2 + (1/r)\partial(r\partial T/\partial r)/\partial r + (1/r^2)\partial^2 T/\partial\Phi^2] + C_A(-\Delta H)k_o \exp(-E/R_gT) \quad (1)$$

Mass balance:

$$\partial C_A/\partial t = k_o \exp(-E/R_gT)\, C_A \quad (2)$$

Initial conditions

$$t = 0: T = T_{in}, C_A = C_{in} \quad (3)$$

and

Boundary conditions

$$0 \leq t \leq t_{ign}$$
$$z = 0: -\lambda\partial T/\partial z = q(r) + h(T - T_{in}) + \sigma T^4$$
$$q(r) = (1-\eta)(2I_o/\pi r_{spot}^2)\exp(-2r^2/r_{spot}^2)$$
$$r = 0: \partial T/\partial r = 0$$
$$r = R: -\lambda\partial T/\partial r = h(T - T_{in}) + \sigma T^4$$
$$z = \infty: -\lambda\partial T/\partial z = h(T - T_{in}) + \sigma T^4 \quad (4)$$

and

$$T(z, r, \Phi) = T(z, r, \Phi + 2\pi)$$

The spatial derivatives are approximated by a second-order centered finite differences, and the integration in time is implicit first order. The computer code used for the simulations performs automatic time step adjustment (Degreve et al., 1987a), spatial mesh adaption (regridding) (Degreve et al., 1987b; Brackbill and Saltzman, 1982), and location of the moving front caused by ablation of material for the heated surface. For a brief description of the computer codes, see the Appendix.

Preliminary findings

An SHS reaction can take place in two combustion propagation regimes: constant pattern and oscillatory. A criterion formulated in Shkadinskii et al. (1971) is:

$$\alpha_c = (RT_{ad}/E)(9.1C_p\, T_{ad}/(-\Delta H) - 2.5) \quad (5)$$

is used to delineate the boundary between the steady-state and oscillating regimes, such that:

$\alpha_c \geq 1$ for steady-state combustion

$\alpha_c < 1$ for oscillatory combustion

For the systems Ti+C and Zr+C simulated in the present study, the values of α_c are 1.4 and 1.2, respectively. Therefore, the combustion of these systems is steady, and we are able to define:

1. Ignition time as the minimum lasing time needed to initiate a self-sustaining reaction front.
2. Ignition temperature as the temperature of the front surface at ignition time.
3. Propagation velocity as the velocity of the plane for which the conversion is 0.5.

The physical properties for the Ti+C and Zr+C systems were obtained from Hardt and Phung (1973), Hardt and Holsinger (1973), and Touloukiam and Ho (1970).

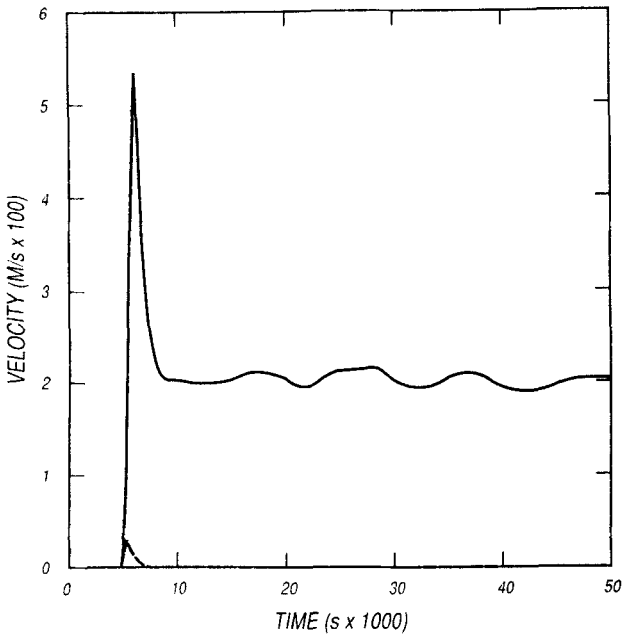

Figure 8. Propagation velocity vs. time for a ZrC sample and heat flux of 6.7 × 10^7 W/m^2.

The solid times for a lasing time which is at most 1 × 10^{-3} s longer than the critical lasing time. The broken line as for a lasing time which is at most 1 × 10^{-3} s shorter than the critical lasing time.

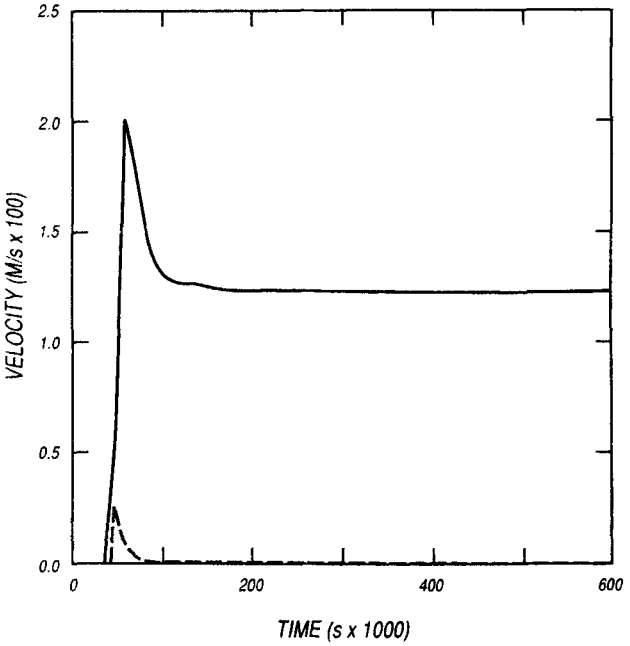

Figure 9. Propagation velocity vs. time for a TiC sample and heat flux of 5.3 × 10^7 W/m^2.

Numerical Results

One-dimensional simulations

In this section, the results of the simulations in one spatial dimension (axial), using the model described above and neglecting variations of temperature and concentration in the other two spatial dimensions (radial and angular), are presented. The propagation velocity of the reaction front is recorded during the lasing process. The propagation velocity attains a constant value after it passes through a maximum (Figures 8 and 9). Initiation of the reaction is achieved only for lasing times longer than the time at which the maximum velocity occurs. This critical time is the ignition time, which depends upon the heat flux. In fact, it is found that

$$t_{ign} \simeq (\text{heat flux})^{-k} \qquad (6)$$

where k = 1.2 for TiC and k = 1.5 for ZrC (Figure 10). This result is in agreement with results presented by Phung and Hardt (1974). Empirically, we find that the peak in the velocity profile coincides with the ignition of the system. Already this provides numerical evidence that abrupt changes do occur in the ignition regime which might be experimentally observable. Also, ignition temperatures are found to be in the range 4,000–8,000 K for both systems.

Obviously, such temperatures are unphysical for this system, primarily because the effect of material ablation during the ignition process is not taken into account here. Inclusion of this effect and comparison of the results with experiments are made in another section.

Two-dimensional simulations

In two-dimensional simulations, the model described in Eqs. 1–4, which neglect variations of temperature and concentration in the angular direction, is used. The laser is focused in the center of the front of the cylindrical sample. The laser power input in the radial direction, which follows a normal distribution, is given by:

$$q(r) = (1 - \eta)\,(2I_o/\pi r_{spot}^2)\exp(-2r^2/r_{spot}^2) \qquad (7)$$

where η is the reflectivity, which is the ratio of the energy reflected from the heated surface (total hemispherical reflectance) to the laser energy output. The average value of η which

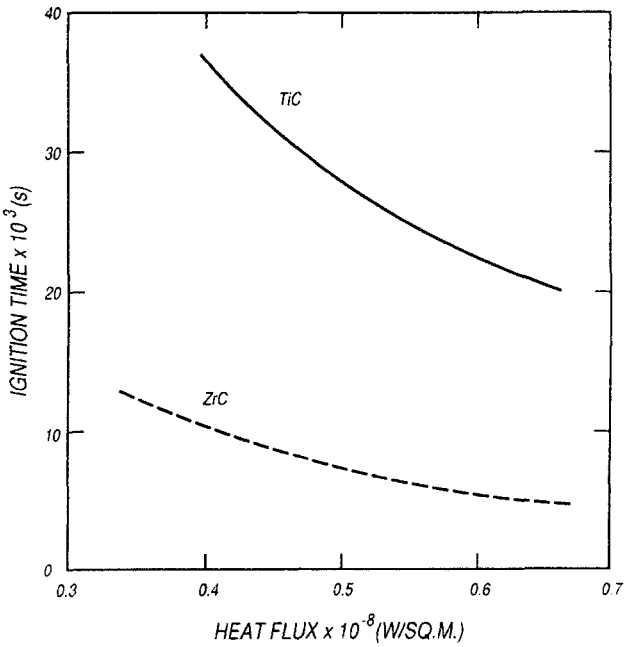

Figure 10. Ignition time vs. heat flux in one dimension.

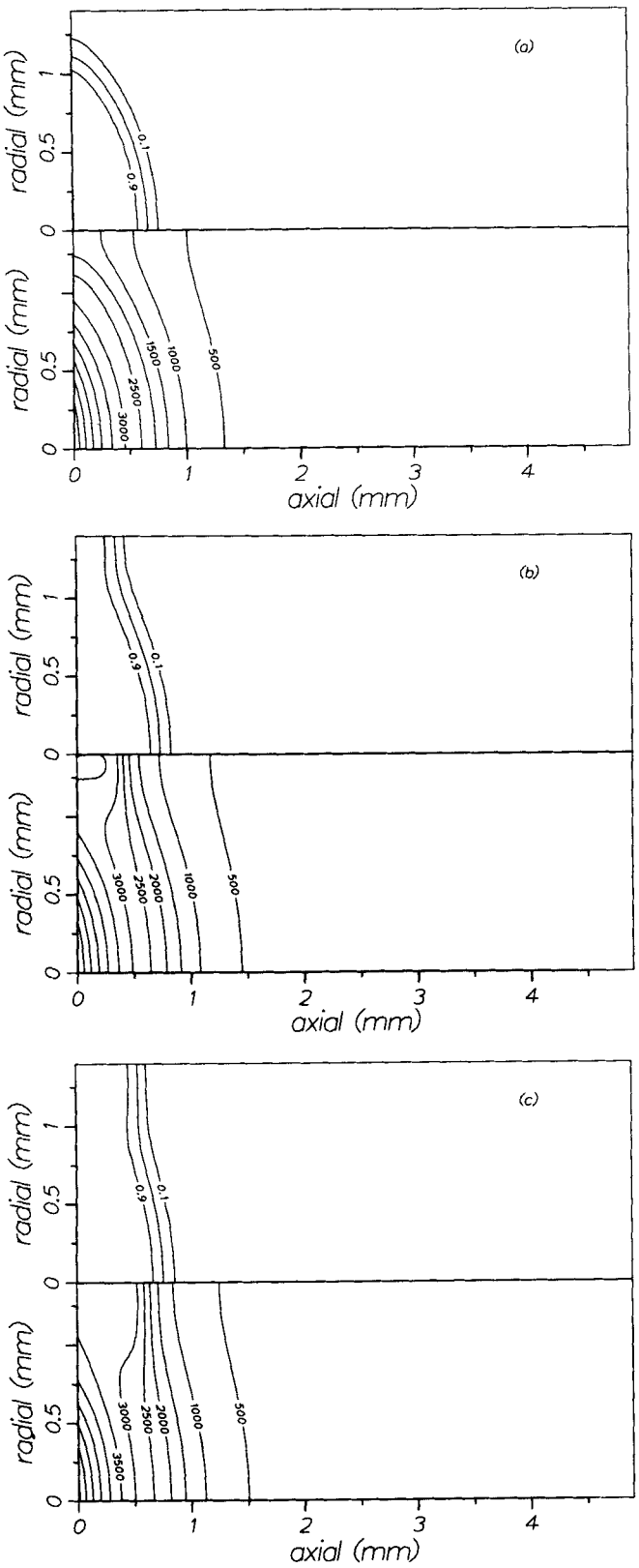

Figure 11. Conversion (upper) and temperature (lower) profiles for a TiC sample at time:

a. 84.2 × 10⁻³ s

b. 101.1 × 10⁻³ s

c. 109.5 × 10⁻³ s

Axes not in proper proportion.

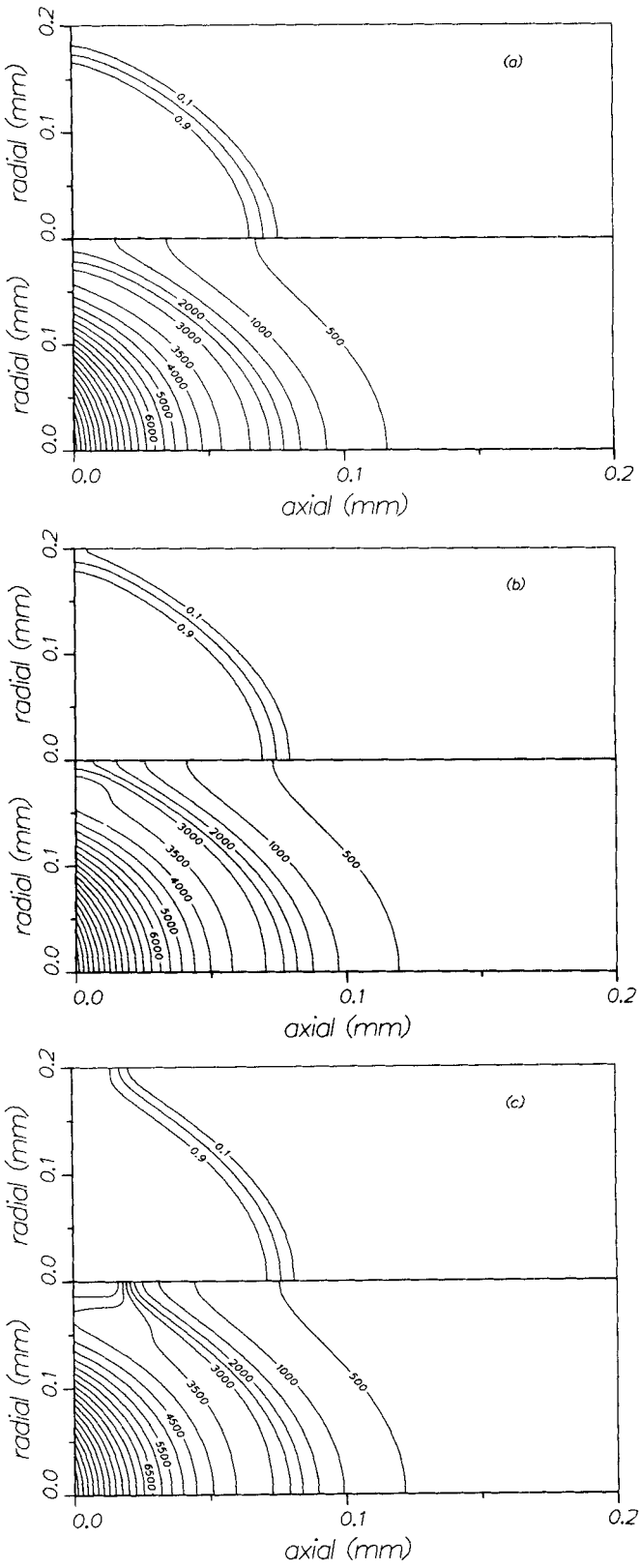

Figure 12. Conversion and temperature profiles for a ZrC sample at time:

a. 2.5 × 10⁻³ s

b. 2.6 × 10⁻³ s

c. 2.7 × 10⁻³ s

Axes not in proper proportion.

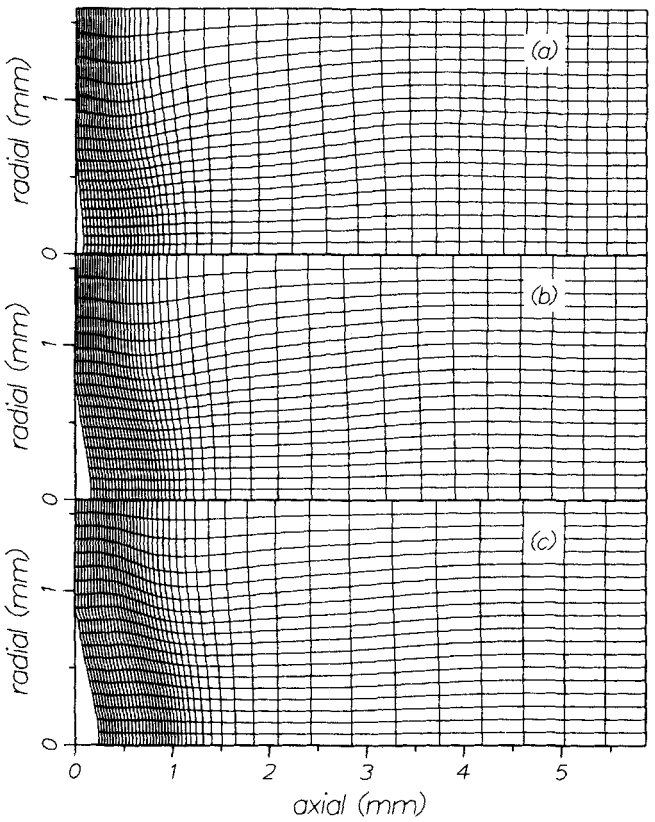

Figure 13. Sample shape at time:
a. 56.2 × 10⁻³ s
b. 112.3 × 10⁻³ s
c. 133.7 × 10⁻³ s
Axes not in proper proportion.

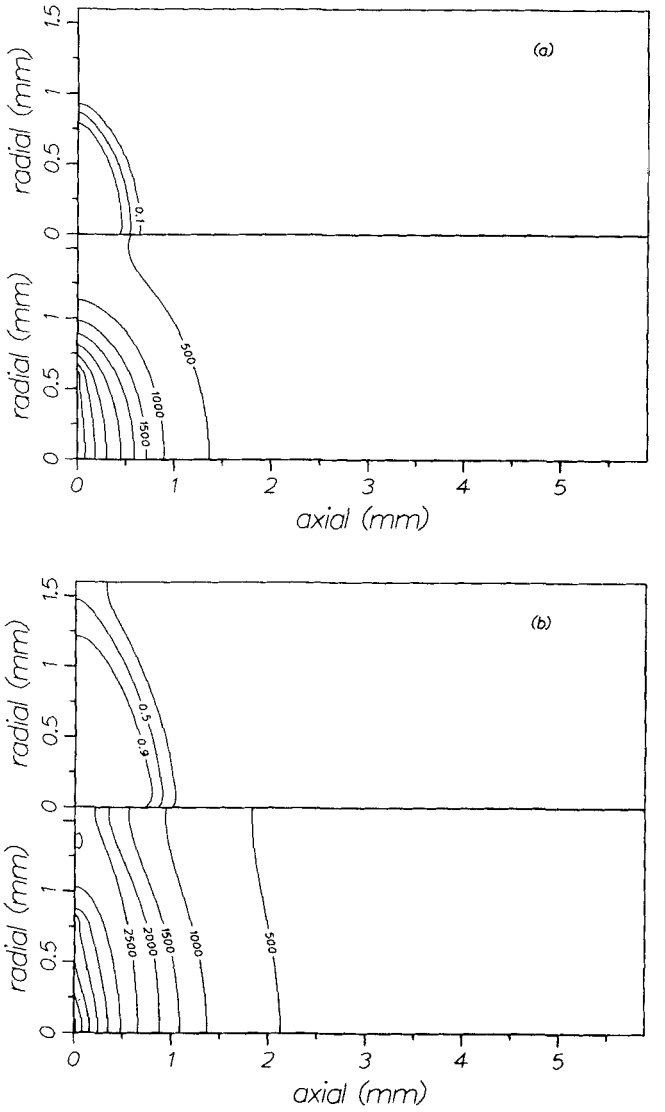

Figure 14. Conversion and temperature profiles at time:
a. 56.2 × 10⁻³ s
b. 168.5 × 10⁻³ s
Axes not in proper proportion.

was used in the calculations was 0.5. Ranges of the data (sample dimensions, density, laser spot size, and power output) taken from Hansen et al. (1987) are presented in Table 1. It should be mentioned that in all 20 simulations, reradiative heat losses from the front and side surfaces are taken into account.

From two sets of results corresponding to the ignition of TiC (Figure 11) and ZrC (Figure 12), two interesting observations can be made. First, a temperature peak appears at the edge of the front surface which is reminiscent of the thermal and velocity spikes found in the 1D simulations. Secondly, since the temperatures obtained at the front surface inside the spot area during the ignition are actually much higher than the sublimation temperatures of TiC and ZrC, a more realistic approach to the ignition process should take into account the additional energy-dissipative mechanisms of melting and ablation.

The effect of melting during the initiation process is studied using the enthalpy method (Voller and Gross, 1981; Puszynski et al., 1985). The inclusion of melting resulted in a lower temperature inside the laser spot. However, this temperature is still very high and the resulting temperature profiles are similar to those in Figures 11 and 12. Absorption of laser radiation leads to material removal from the heated surface (Ready, 1964; Beiko et al., 1967; Crane et al., 1980; Klein and Berry, 1987; Rycalin and Uglov, 1982) due to product sublimation and particle ejection. The location of the moving front surface due to material removal is found either by estimating a sublimation rate based on the latent heat of sublimation or by using an effective material removal rate estimated from the experimental data. In either approach, the materials removal rate follows a normal distribution on the front surface. A brief description of the code used is presented in the Appendix.

Initially, it is assumed that material removal takes place at a constant sublimation temperature, T_v, which is approximately 4,000 K and 4,900 K for TiC and ZrC, respectively, at 10^5 Pa

Table 3. Ignition Times for Laser Power of 77 W

Samples	Material Removal	Ignition Time s × 10^{-3}
S1	No	98
	Yes	125
S2	No	112
	Yes	145

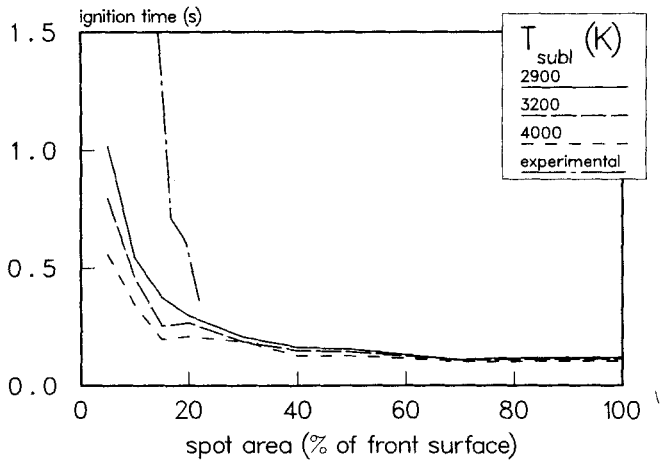

Figure 15. Ignition times vs. laser spot area for Ti+C pellet with total front surface area of 5.72 × 10^{-4} m^2 and average total laser power of 77 W.

pressure. The results obtained from the sublimation of the ignition of a TiC sample—5 × 10^{-3} m long, 2.5 × 10^{-3} m dia., and 3.36 × 10^3 kg/m^3 in are presented in Figure 13 (sample shape) and Figure 14 (temperature and conversion profiles). In Table 3, ignition times for average laser power of 77 W, and spot areas 50% and 15% of the front surface area for samples S1 and S2 are given. The ignition times obtained are 25% longer than the ones obtained when material removal is neglected.

The effect of the laser spot area, for a constant average laser power on the ignition time, is studied for a TiC sample of 2.6 × 10^{-3} kg/m^3 in density, 2.7 × 10^{-3} m dia., and average laser power of 77 W, and the results are presented in Figure 15. As can be seen, the minimum ignition time is obtained for a laser spot area covering 75% of the total front surface area at this power and for these sample characteristics.

During the experiments, the laser power is observed to fluctuate by ±10% around the average power with an approximate period of 5 × 10^{-3} s. Taking these power fluctuations into account, the ignition of the same TiC sample (d = 2.7 × 10^{-3}

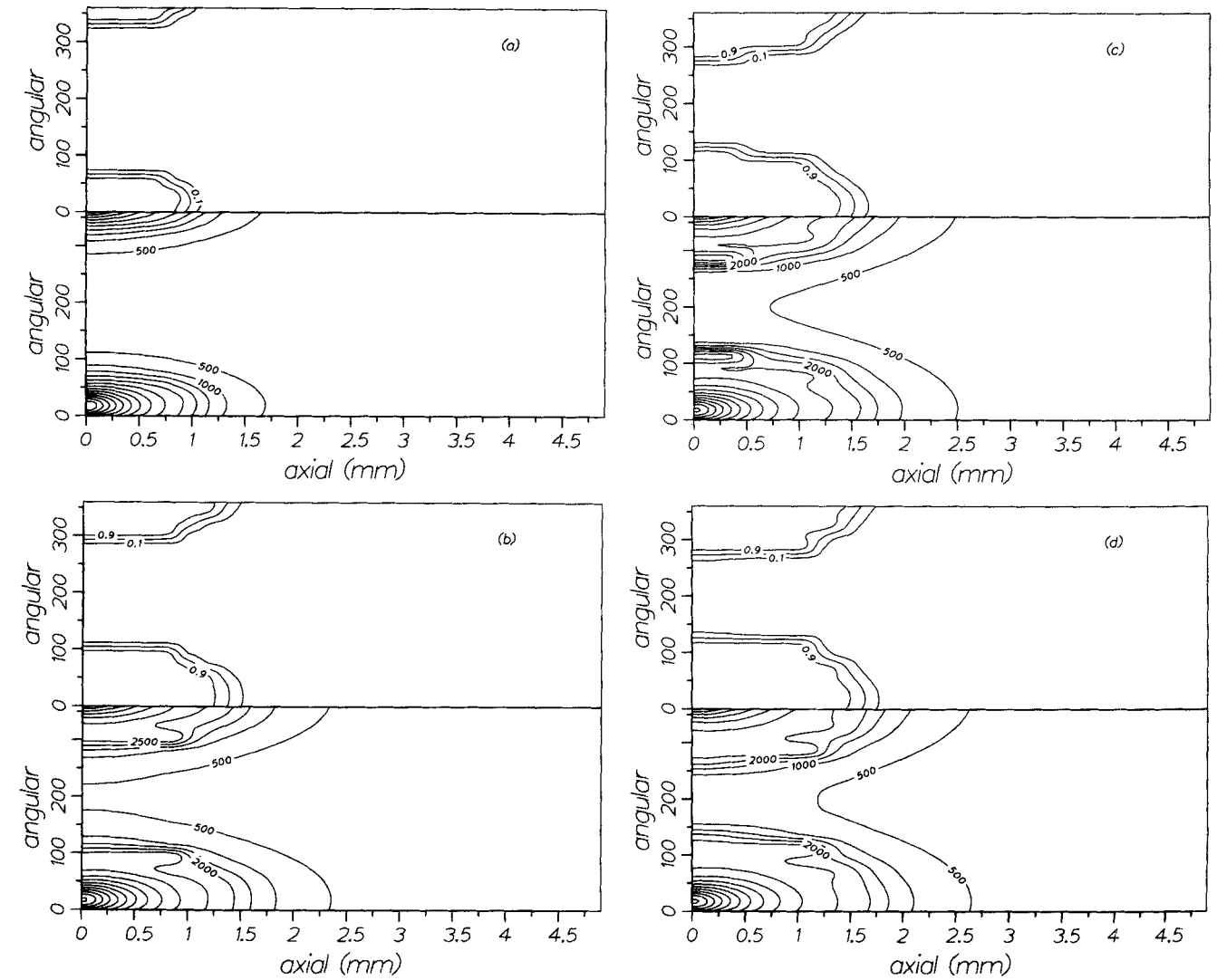

Figure 16. Conversion and temperature profiles at the lateral surface of the sample at time:

a. 112.3 × 10^{-3} s

b. 224.0 × 10^{-3} s

c. 252.7 × 10^{-3} s

d. 290.3 × 10^{-3} s

Axes not in proper proportion.

m) is simulated. The minimum ignition time is obtained for a laser spot area which is still 75% of the front surface area and ignition is delayed by 0.005 to 0.008 s.

The two-dimensional simulations reveal that the ignition process depends mainly on the energy deposited in the system. The time to ignition is longer for higher heat fluxes keeping the average laser power constant, since much of the energy is reradiated from the heated surface or consumed during the process of material removal. From Figure 15, it is evident that for very small spot sites, <10%, the model for material removal is not nearly efficient enough. While the general trend is correct, the ignition times at spot sizes around 5% are much longer experimentally. One possible source of discrepancy between the model and the experiment may be that, at smaller spot sizes, the detailed structure of the laser power density profile may become important. Another reason may be that estimation method of the effective heat of ablation or material removal may need to be revised. Finally, we note that the experimental ignition times are upper bounds to the ignition times as defined above.

Three-dimensional simulations

In the three-dimensional simulations, the full model described by Eqs. 1–4 is used. The effect of focusing the laser outside the center of the front surface is studied for the ignition of the same TiC sample used in the study of the optimum laser spot size, and the results are presented in Figure 16. The laser spot is located 5×10^{-4} m from the center of the front disk, and the laser spot area covers 10% of the front surface area. The conversion and temperature profiles presented correspond to those found at the lateral surface of the cylindrical sample roughly corresponding to what might be observed through a series of pyrometer readings. The ignition time is 35% longer than the ignition time found in the two-dimensional simulations (laser spot located in the center of the front disk). Also, as can be seen in Figure 14, the conversion and temperature profiles during the ignition process are not planar. Since the systems studied exhibit steady combustion, these profiles will eventually become planar. However, for systems which can exhibit oscillatory combustion, focusing the laser outside the center of the front surface results in symmetry breaking and generates traveling hot spots (Figure 17). Therefore, a more accurate study of the laser ignition process, and later, of the front propagation requires the use of the full three-dimensional model. Here, note that at least some aspects of the low symmetry behavior of solid-state combustion are now obtainable.

Conclusions

During ignition, the temperature jump, which is observed experimentally inside the heated spot, is much lower than the adiabatic temperature rise. This implies that the extent of the reaction in the spot, prior to ignition, is significant. The fact that the conversion is nonzero inside the spot area is also supported by the numerical calculation (Figures 9 and 10). Also, as can be seen from these figures, a high-temperature jump takes place at ignition on the edge of the front surface. This temperature peak, which is reminiscent of the thermal and velocity spikes found in the 1D simulations, can also be used to determine the ignition time if the pyrometer is aimed there. The ignition temperatures, observed during the experiments, are in very good agreement with those calculated in all dimensions. The shape of the reaction zone in two and three dimensions is always nonplanar for

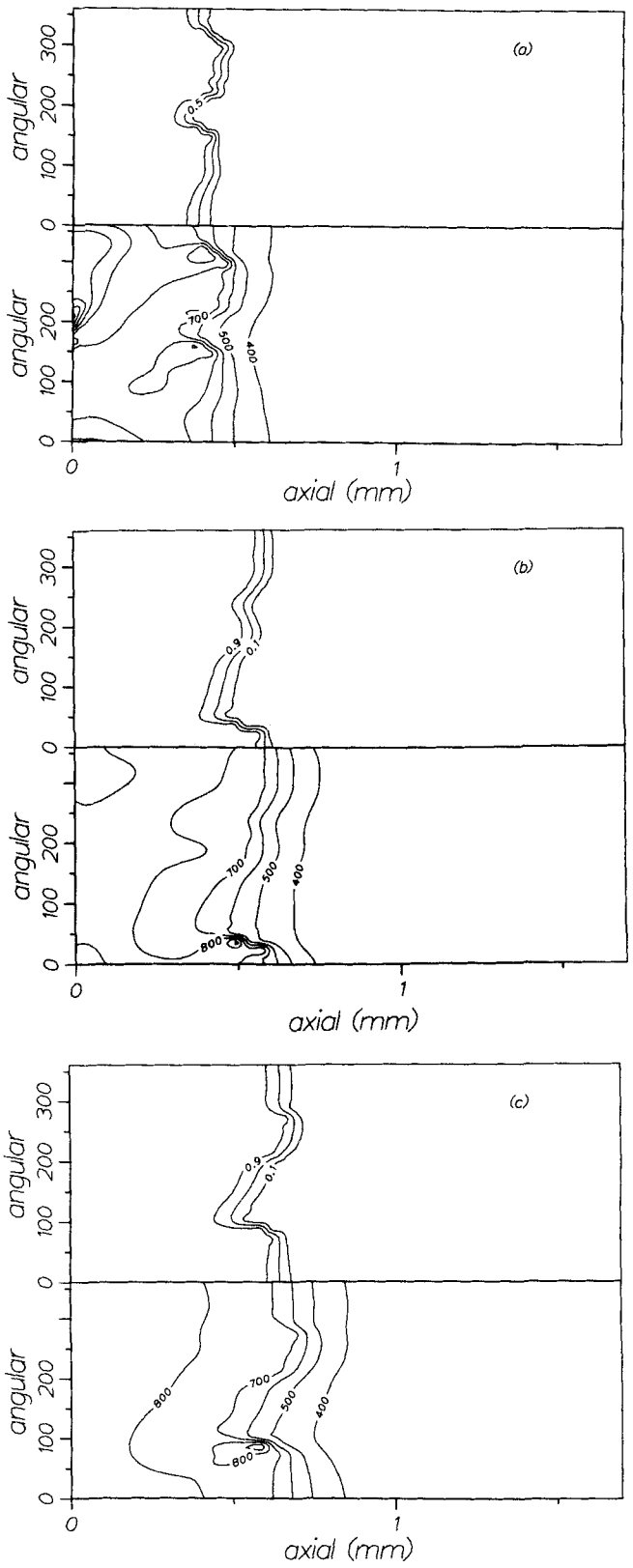

Figure 17. Conversion and temperature profiles at the lateral surface of the sample at time:
a. 21.8 × 10⁻³ s
b. 25.4 × 10⁻³ s
c. 29.0 × 10⁻³ s
Axes not in proper proportion.

the systems considered, indicating, as in the experiments, that the ignition regime is very far from the steady regime in these systems.

The ignition times obtained from the 2D simulations are in the range of 0.1 to 1.0 s, which is in agreement with the calculated ignition times by Borokovi et al. (1986), using a similar approach. The experimental ignition times range from 0.3 to 10 s depending on the spot size and average laser power. In the regime where material removal is not too important, relative spot size greater than 10%, the agreement between experiment and numerical simulation is reasonably good. For smaller spot sizes, the experimental ignition times become much longer than the calculated ones. The two main concerns on this point are: 1) whether the model for material removal used in the simulations is efficient enough and 2) whether the pyrometry signatures used to indicate ignition are still valid for these conditions.

Finally, for a given laser output, there is a laser spot area, as a percentage of the front surface, for which the minimum ignition time is attained. This is 75%, in the calculations performed in the course of the present work. The simulations also suggest that aiming the front surface pyrometer at the edge of the sample may be preferable to timing it in the laser spot.

The 3D simulations reveal that the ignition time increases when the laser is focused outside the center of the front surface. Also, focusing of the laser outside the center can lead to traveling hot spots, if the system to be ignited can exhibit an oscillating propagation front (Figure 17).

Notation

C_A = concentration
C_p = heat capacity
E = activation energy
h = heat transfer coefficient
I_o = average laser power
k_o = reaction rate constant
q = heat flux
r = radial coordinate
R_g = gas constant
t = time
T = temperature
z = axial direction

Greek letters

α = parameter appearing in Eq. 5
ΔH = heat of reaction
λ = thermal conductivity
ρ = density
σ = radiation coefficient
Φ = angular direction
η = reflectance

Subscripts

in = initial
ign = ignition
spot = lower spot, normal laser spot radius

Literature Cited

Assovskii, I. G., and O. I. Leipunskii, "Theory of Ignition of Fuels by Light Pulses," *Fiz. Gor. Vzryva*, **16**(1), 3 (1980).

Baranovskii, A. M., "Laser Ignition of Pressed Composites," *Fiz. Gor. Vzryva*, **19**(3), 95 (1983).

Boroskoi, I. B., S. S. Bondarchuk, E. A. Kotlov, and V. N. Vilyunov, "Solving the Problem of Condensed System Ignition on the Basis of a Difference Scheme with a Calculation Grid Which Varies over Time," *Fiz. Gor. Vzryva*, **22**(3), 14 (1986).

Brackbill, J. V., and J. S. Saltman, "Adaptive Zoing for Singular Problems in Two Dimensions," *J. Comp. Phys.*, **46**, 342 (1982).

Crane, K. C. A., R. K. Garnsworthy, and L. E. S. Mathias, "Ablation of Materials Subjected to Laser Radiation and High-Speed Gas Flows," *J. App. Phys.*, **51**(11), 5954 (1980).

Degreve, J., P. Dimitriou, J. Puszynski, and V. Hlavacek, "Modeling of Strongly Exothermic Reactions on a Supercomputer," *Chem. Eng. Comm.*, **58**, 105 (1987a).

Degreve, J., P. Dimitriou, J. Puszynski, V. Hlavacek, S. M. Valone, and R. G. Behrens, "Use of 2D Adaptive Mesh in Simulation of Combustion Front Phenomena," *Comp. Chem. Eng.*, **11**, 749 (1987b).

Fredin, L., G. P. Hansen, M. P. Sampson, J. L. Margrave, and R. G. Behrens, "A High Temperature Quadrapole Mass Spectrometer for Studying Vaporization from Material Heated by a CO_2 Laser," Los Alamos National Laboratory, Report No. LA-UR-2053 (1987).

Hardt, A. P., and R. W. Holsinger, "Propagation of Gasless Reactions in Solids: II. Experimental Study of Exothermic Intermetallic Reaction Rates," *Comb. Flame*, **21**, 91 (1973).

Hardt, A. P., and P. V. Phung, "Propagation of Gasless Reactions in Solids: I. Analytical Study of Exothermic Intermetallic Reaction Rates," *Comb. Flame*, **21**, 77 (1973).

Klein, C. A., R. F. Menefee, B. D. Krenek, and M. J. Berry, "Small-Scale Laser Effects Experiments on Graphite: Coupling Coefficient, Lateral Loss, and Effective Heat of Ablation," *J. Appl. Phys.*, **11**, 1701 (1987).

Korotkevich, I. I., G. V. Khil'echenko, G. P. Polunina, and L. M. Vidaskii, "Initiation of Self-Propagating High-Temperature Synthesis Reactions by Pulsed Laser Radiation," *Fiz. Gor. Vzryva*, **17**(5), 61 (1981).

Merzhanov, A. G., and A. E. Averson, "The Present State of the Thermal Ignition Theory: An Invited Review," *Comb. Flame*, **16**, 89 (1971).

Micheev, V. F., A. A. Koval'skii, and S. S. Khlevnoi, "Ignition of a Ballistics Propellent by Light Radiation," *Fiz. Gor. Vzryva*, **4**(1), 3 (1968).

Phung, P. V., and A. P. Hardt, "Ignition characteristics of Gasless Reactions," *Comb. Flame*, **22**, 323 (1976).

Puszynski, J., V. K. Jayaraman, and V. Hlavacek, "A Stefan Problem for Exothermic Noncatalytic Reactions," *Int. J. Heat Mass Transfer*, **29**(6), 1237 (1985).

Ready, J. F., "Effects due to Absorption of Laser Radiation," *J. Appl. Phys.*, **36**(2), 462 (1964).

Rycalin, N. N., and A. A. Uglov, "Thermophysical Processes in the Interaction of Laser Radiation with Absorbing Media," *Izv. Akad. Nauk SSSR*, **46**(6), 1018 (1982).

Shkadiskii, K. G., B. I. Kaihakin, and A. G. Merzhanov, "Propagation of a Pulsating Exothermic Reaction Front in the Condensed Phase," *Fiz. Gor. Vzryva*, **7**(1), 19 (1971).

Stovbun, V. P., T. I. Kedrova, and V. V. Barzykin, "Ignition of Systems with High-Melting Reaction Products," *Fiz. Gor. Vzryva*, **8**(3), 349 (1972).

Touloukian, Y. S., and C. Y. Ho, *Thermophysical Properties of Matter*, **1, 2**, Plenum Press, New York (1970).

Veiko, V. P., Ya. M. Imas, A. N. Kokora, and M. M. Libenson, "Metal Temperature in Interaction Region with a Laser Beam," *Zh. Tekhn. Fiz.*, **37**(10), 1920 (1967).

Vidavskii, L. M., G. B. Khil'chenko, I. I. Kortokevich, G. P. Polunina, and V. I. Spitsyn, "Thermal Initiation of Chemical Reactions by Powerful Light Pulses," *Dokl. Akad. Nauk SSSR*, **219**(5), 1157 (1974).

Vilyunov, N. Y., "On the Thermal Theory of Ignition," *Fiz. Gor. Vzryva*, **2**(2), 77 (1966).

Voller, V., and M. Cross, "Accurate Solutions of Moving Boundary Problems Using the Enthalpy Method," *Int. J. Heat Mass Transf.*, **24**, 545 (1981).

Zarko, V. E., and A. B. Kiskin, "Numerical Modeling of Nonsteady Powder Combustion under the Action of a Light Flux," *Fiz. Gor. Vzryva*, **16**(6), 54 (1980).

Appendix: Structure of the Code

The code is described briefly by the following steps:

Step 1. Solve energy and mass balances at time t.

Step 2. Locate points of the front surface for which $T \geq T_v$.

Step 3. For those points, set the temperature to T_v and move them according to Procedure 1 or 2 described below.

Step 4. Calculate the new temperature and conversion profiles (interpolation).

Step 5. Call routine for spatial mesh adoption.

Step 6. $t = t + \Delta t$

Step 7. If $t \leq$ maximum time of integration, repeat Steps 1 to 6; otherwise, stop.

In Step 3 above, one of two procedures is used to move the solid surface, when material removal has occurred.

Procedure 1. At time t, the initial sublimation rate used is the sublimate rate estimated at time $t = \Delta t$. The sublimation rate is estimated through iterations between Steps 1 and 5. The iterations continue until the criterion $1 - \epsilon < E_a/E_b < 1 + \epsilon$ is satisfied.

where

E_a = energy input (laser) + energy released (reaction)

E_b = energy required for a sublimation + energy increase of the system

ϵ = small number (10^{-2})

At each iteration, the sublimation rate is corrected by the ratio: E_a/E_b. It is observed that, after a few steps, the sublimation rate reaches a constant value, although one call to the mesh adoption routine each time is still required.

Procedure 2. An effective material removal rate, corresponding to the center of the front disk, is estimated from the experimental data as follows:

$$\text{sublimation rate} = \frac{\text{height of the cone created}}{\text{lasing time}}$$

The estimated rate is kept constant throughout the ignition process. (No iterations are needed.)

Procedure 1 is very expensive because of the calls to the adaptive routine after each iteration. Therefore, Procedure 2 is used during the simulations. Also, it should be mentioned that, in either approach, the material removal rate follows a normal distribution in the radial direction on the front surface.

The algorithms used for the equation of change integration and the automatic time step adjustment are described in Degreve et al. (1987a).

Manuscript received Dec. 2, 1987, and revision received Apr. 6, 1989.